

PrBi, a semimetal where topology meets quadrupolar degrees of freedom

Xiaobo He¹, Chuanwen Zhao², Haiyang Yang³, Jinhua Wang¹,
Kangqiao Cheng¹, Shan Jiang¹, Lingxiao Zhao¹, Yuke Li³, Chao
Cao³, Shun Wang², Zengwei Zhu¹, Yongkang Luo^{1*}, and Liang Li¹

¹*Wuhan National High Magnetic Field Center and School of Physics,
Huazhong University of Science and Technology, Wuhan 430074, China;*

²*MOE Key Laboratory of Fundamental Physical Quantities Measurement &
Hubei Key Laboratory of Gravitation and Quantum Physics, School of Physics,
Huazhong University of Science and Technology, Wuhan 430074, China; and*

³*Department of Physics and Hangzhou Key Laboratory of Quantum Matters,
Hangzhou Normal University, Hangzhou 311121, China.*

(Dated: September 11, 2019)

* Electronic address: mpzslyk@gmail.com

Novel materials incorporating electronic degrees of freedom other than charge, including spin, orbital and valley *et al* have manifested themselves to be of the great interests and applicable potentials. Recently, the multipolar degrees of freedom have attracted extensive attention in the electronic correlated effects. In this work, we systematically studied the transport, magnetic and thermodynamic properties of the topological semimetal candidate PrBi in the framework of crystalline electric field theory. Our results demonstrate the Γ_3 non-Kramers doublet as the ground state of Pr^{3+} ($4f^2$) ions. This ground state is nonmagnetic but carries a non-zero quadrupolar moment $\langle \hat{O}_2^0 \rangle$, and the latter is inferred to undergo a quadrupolar phase transition below 0.08 K. No obvious quadrupolar Kondo effect can be identified. Ultrahigh-field quantum oscillation measurements confirm PrBi as a semimetal with non-trivial Berry phase and low total carrier density 0.06 /f.u. We discuss the interplay between low carrier density and $4f^2$ quadrupolar moment, and ascribe the weak quadrupolar ordering and Kondo effect as consequences of the low carrier density. PrBi, thus, opens a new window to the physics of topology and strongly correlated effect with quadrupolar degrees of freedom in the low-carrier-density limit, evoking the need for a reexamination of the Nozières exhaustion problem in the context of multi-channel Kondo effect.

INTRODUCTION

Kondo effects involving quadrupolar degrees of freedom have attracted extensive attention. A conventional Kondo effect[1, 2] depicts that the magnetic moment (spin, *i.e.* dipolar degrees of freedom) of a spin-1/2 impurity immersed into the sea of conduction (*c*) electrons is screened and quenched by forming an entangled Kondo singlet[3]. On the other hand, magnetic exchanges between these local moments can be realized via the so-called Ruderman-Kittel-Kasuya-Yosida (RKKY) interaction which is also mediated by the conduction electrons[4–6]. The competition between Kondo effect and RKKY interaction leads to a quantum critical point[7] in the vicinity of which many emergent quantum phenomena may appear, such as heavy-fermion, non-Fermi liquid, unconventional superconductivity and so on. Theories have also suggested that nonmagnetic Kondo effect can also be realized by taking the multipolar degrees of freedom. Cox proposed that f^2 ions like Pr^{3+} or U^{4+} sitting

in a cubic-symmetrized crystalline electric field (CEF) may have Γ_3 nonmagnetic doublet ground state whose *quadrupolar moment* can interact with conduction electrons[8, 9], termed as *quadrupolar Kondo effect*. Likewise, indirect RKKY-like interaction was also proposed to play an essential role to mediate the long-range quadrupolar ordering[10, 11]. A variety of interesting properties associated with the quadrupolar degrees of freedom have been observed, see for examples the Pr-based intermetallic family $\text{Pr}Tm_2X_{20}$, where $Tm=\text{Ti}, \text{V}, \text{Rh}, \text{Ir}$, and $X=\text{Al}, \text{Zn}$ [12–17].

For whatever dipolar or quadrupolar Kondo effect, a general presumption is that the system contains indefinitely sufficient conduction electrons to screen the local moments. An interesting question, then, is what if in a system with low carrier density? This encourages us to recall the famous Nozières exhaustion idea[18] that an insufficient number of conduction-electron spins to separately screen a large amount of local moments. In the dipolar Kondo compounds $\text{Yb}XCu_4$ ($X=\text{Ag}, \text{Au}, \text{Cd}, \text{Mg}, \text{Tl}$, and Zn), this idea has been testified by the fact that the development of Kondo coherence is severely protracted as carrier density decreases[19, 20]; whereas the similar question remains open in the quadrupolar Kondo effect. Intuitively, carrier density should be even more critical for the quadrupolar Kondo effect, because here the Kondo effect is multi-channel and thus requires an *over-screening* number of conduction electrons. The condition on the RKKY side is equally interesting. Because low carrier density means a dearth of conduction electrons to transfer the RKKY interaction, the long-range ordering is expected to be weakened, too. A further question one may pose is, on the whole, how does the low carrier density affect those emergent phenomena involved by quadrupolar degrees of freedom? To answer these questions, proper material basis with f^2 ions in cubic site symmetry, and most importantly, of low carrier density, are needed.

In this work, we systematically studied the physical properties of the cubic-structured semimetal PrBi . Previous studies on PrBi have reported a large magnetoresistance (MR) which potentially originates from electron-hole compensation[22, 23]. Herein, the quantum oscillation measurements up to 53 T not only find the low carrier density of ~ 0.06 /f.u., but also points to a topologically non-trivial Berry phase. The magnetic and thermodynamic properties of PrBi are well understood in the framework of CEF theory. We demonstrate that the CEF ground state of $\text{Pr}^{3+} 4f^2$ electron is a nonmagnetic Γ_3 doublet whose quadrupolar moments likely form a quadrupolar ordering below 0.08 K. The influence of low

carrier density on the correlation effect involving quadrupolar degrees of freedom is discussed.

RESULTS

The compound studied here, PrBi, is a topological semimetal with low carrier density. This can be seen from the transport measurements as shown in Fig. 1. The sample measured is of good quality, guaranteed by the large residual resistance ratio (RRR) about 151, comparable to previous reports[22, 23]. Over the full range 2-300 K, we did not see any anomaly or in particular any trace of $-\log T$ behavior in $\rho_{xx}(T)$ as seen in some Pr-based intermetallic compounds[15]. This implies that quadrupolar Kondo effect arising from *c-f* hybridization is weak for temperature above 2 K. Under magnetic field and at low temperature, it exhibits extremely large magnetoresistance, as commonly seen in many other semimetals[25]. At 2 K, the MR reaches 440,000% (20,000%) for field up to 53 T (9 T). The nearly parabolic $\rho_{xx}(B)$ profile and unsaturated MR should be attributed to electron-hole compensation[22, 23, 25, 26].

Clear Shubnikov-de Hass (SdH) quantum oscillations can be seen in $\rho_{xx}(B)$. After subtracting the non-oscillatory background $\langle \rho_{xx} \rangle$, we show the oscillatory part $\Delta\rho_{xx}$ in Fig. 1(c) as a function of $1/B$. The Fast Fourier Transform (FFT) pattern displays multiple frequencies, cf Fig. 1(d) where the de Haas-van Alphen (dHvA) oscillation results of LaBi and PrBi are also presented for comparison. The quantum oscillation arises from quantized Landau levels passing over the Fermi surface, and the frequency (F) of oscillation in the $1/B$ domain is proportional to the extremum cross-section (S_F) of Fermi surface, $F = \frac{\hbar}{2\pi e} S_F$. The Fermi surfaces of PrBi calculated by the DFT are displayed in Fig. 2(a). It consists of two hole pockets (β and γ) co-centered at Γ , and three electron pockets (α) located at \mathbf{X} . Following the same notation in LaBi[21], the two fundamental frequencies $F=255$ and 560 T are assigned as (vertical) α and β pocket, respectively. In addition, there is a small peak at 1511 T. By comparing with LaBi[21], this frequency should originate from those horizontal α pockets whose elongate axes are in \mathbf{k}_x and \mathbf{k}_y so that their cross-sections are much larger. We, therefore, denote it $F_{\alpha'}$. The topology of the Fermi surfaces can be mapped out by angular dependent SdH measurements [Fig. 1(e)]. As expected, F_β is essentially independent with field angle, consistent with a nearly spherical shape. F_α , in contrast, changes slowly for small angle, but increases rapidly for angles larger than 45° , in agreement with the calculated ellipsoidal character. It should be pointed out that $F_{\alpha'}$ is hardly seen between

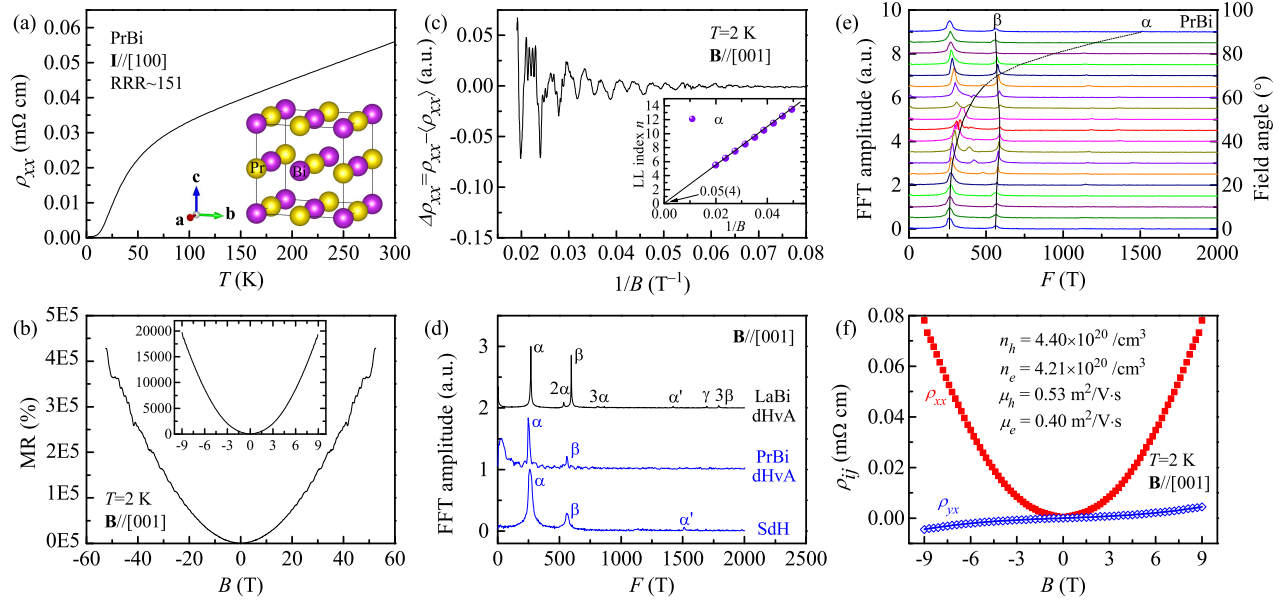


FIG. 1: **Electrical transport properties of PrBi.** (a) Resistivity as a function of temperature, $\rho_{xx}(T)$, in the absence of magnetic field. (b) MR reaches 430,000% (20,000%) for field up to 53 T (9 T). (c) SdH oscillation in $\Delta\rho_{xx}$ as a function of $1/B$. The inset depicts the Landau-level fan plot. The intercept at infinite-field limit indicates non-trivial Berry phase. (d) FFT of dHvA and SdH oscillations of PrBi (blue) and LaBi (black). (e) SdH FFT of PrBi for various field orientations, $\mathbf{B} \perp \mathbf{I}$. The black lines are guide lines to the Fermi surface structure. The dotted line is speculated from DFT calculations[21]. (f) $\rho_{xx}(B)$ and $\rho_{yx}(B)$ measured at 2 K. The solid line represents the two-band fitting of $\rho_{yx}(B)$.

70 and 85 $^\circ$, similar as the case in LaBi[21]. Moreover, the star-shaped γ pocket is not visible in our SdH measurements for all the field angle. A comparison between calculated and experimental SdH frequencies can be found in Fig. 2(b-c).

The electron carrier density can be calculated by estimating the total volume of α pockets, and this yields $n_e=4.08 \times 10^{20} \text{ cm}^{-3}$. Note that we have incorporated the spin degeneracy. Since F_γ is missing in SdH, we can not obtain the hole carrier density directly, however, n_h is assumed to be close to n_e in semimetals[27]. Such an electron-hole compensation effect can be evidenced by fitting the Hall resistivity $\rho_{yx}(B)$ to a two-band model[26, 27]. We obtain $n_h=4.40 \times 10^{20} \text{ cm}^{-3}$, $n_h=4.21 \times 10^{20} \text{ cm}^{-3}$, and the mobilities $\mu_h=0.53 \text{ m}^2/\text{V}\cdot\text{s}$ and $\mu_e=0.40 \text{ m}^2/\text{V}\cdot\text{s}$ [see Fig. 1(f)]. The total carrier density, n_h+n_e , is about $8.6 \times 10^{20} \text{ cm}^{-3}$,

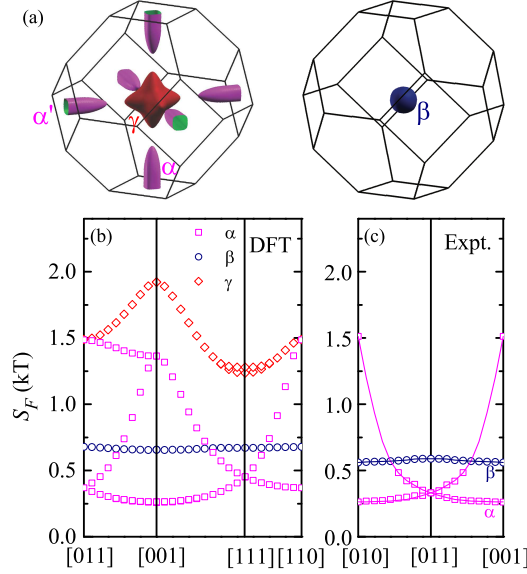


FIG. 2: **Fermi surface of PrBi.** (a) DFT calculated Fermi surface of PrBi. The Fermi surfaces are indexed as α (electron-type, ellipsoidal, at X), β (hole-type, spherical, at Γ), and γ (hole-type, star-shaped, at Γ), respectively. The angular dependence of Fermi surface cross-sections are shown in panels (b) and (c), from theoretical and experimental, respectively.

or equivalently, 0.06 in each PrBi unit cell.

The topological feature can be manifested by the Landau-level (LL) diagram, as shown in the inset to Fig. 1(c). Our pulsed-field measurements up to 53 T enable us to determine the LL index much closer to the quantum limit in good accuracy. Since $\rho_{xx} \gg \rho_{yx}$, ρ_{xx} is in-phase with conductivity σ_{xx} , the minima of $\Delta\rho_{xx}$ should be assigned as half-integer Landau level[28]; this criterion is in line with classic 2D quantum Hall effect[29]. The extrapolation of α -pocket LL diagram to the infinitely large field limit results in an intercept 0.05(4). For a three dimensional Fermi surface, this intercept corresponds to $1/2 - \Phi_B/2\pi - \delta$ [30], where Φ_B is the Berry phase, and $-1/8 \leq \delta \leq 1/8$ is an additional phase shift due to the curvature of the Fermi surface topology. The obtained intercept 0.05(4) falling between $\pm 1/8$ thus manifests a non-trivial Berry phase $\Phi_B=1/2$. Recent DFT calculations on PrBi also suggested bulk band inversion and gapless surface state, further lending support to a topologically non-trivial nature[23].

The main frame of Figure 3 shows the magnetic susceptibility (χ) of PrBi measured with $\mathbf{B} \parallel [001]$. Above 25 K, $\chi(T)$ conforms to the standard Curie-Weiss law $\chi(T) = C/(T - \theta_W)$.

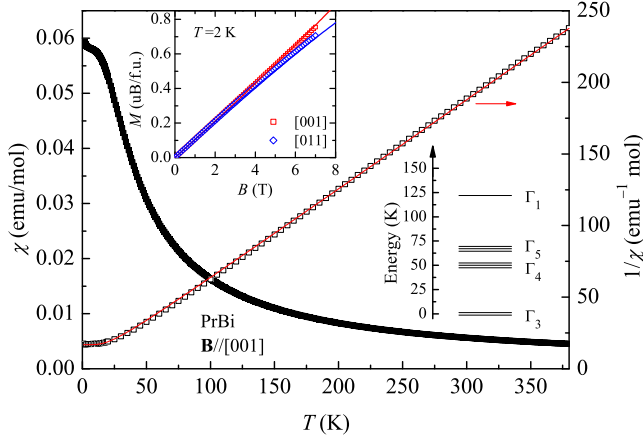


FIG. 3: **Magnetic properties of PrBi.** Temperature dependence of magnetic susceptibility of PrBi measured under $B=0.1$ T and $\mathbf{B}\parallel[001]$. The inverse of χ is shown in the right frame. The symbols stand for experimental data, while the solid lines are theoretically calculated results based on CEF theory. The lower inset depicts the CEF splitting of the $j=4$ multiplet. The upper inset displays the field dependent isothermal magnetization at 2 K for $\mathbf{B}\parallel[001]$ (red squares) and $\mathbf{B}\parallel[011]$ (blue diamonds), respectively.

The derived effective moment is $3.57 \mu_B$, very close to the value for a free Pr^{3+} ion. The fitted Weiss temperature is negligibly small, $\theta_W=-0.5(2)$ K, much smaller than those in other cubic Pr intermetallic compounds, like PrMg_3 (-40 K)[31], $\text{PrOs}_4\text{Sb}_{12}$ (-16 K)[32], $\text{PrTi}_2\text{Al}_{20}$ (-40 K)[15], $\text{PrV}_2\text{Al}_{20}$ (-55 K)[15]. Below 25 K, $\chi(T)$ gradually deviates and tends to saturate, suggestive of a van-Vleck paramagnetic ground state which is a consequence of CEF splitting.

The CEF Hamiltonian for Pr^{3+} in O_h point group (cubic) writes[33, 34]

$$\hat{H}_{CEF} = B_4(\hat{O}_4^0 + 5\hat{O}_4^4) + B_6(\hat{O}_6^0 - 21\hat{O}_6^4), \quad (1)$$

where \hat{O}_l^m ($l=4,6$; $m=0,4$) are Stevens operators[35], and B_4 and B_6 are CEF parameters that can be determined experimentally. The nine-degenerated $j=4$ multiplet of Pr^{3+} in such a CEF splits into one singlet (Γ_1), one doublet (Γ_3) and two triplets (Γ_4 and Γ_5)[36]. It is particularly interesting when the Γ_3 doublet is the ground states, whose quadrupolar degrees of freedom are deemed to be responsible for many emergent quantum phenomena[8].

We demonstrate that Γ_3 is the ground state in PrBi by fitting the magnetic susceptibility to the CEF theory, in which B_4 and B_6 are set as free parameters. The best fitting parameters are $B_4=0.0012(2)$ K, and $B_6=-0.00065(3)$ K. This is equivalent to $W=-0.8911$ K and

TABLE I: CEF parameters, energy levels, wave functions and the $4f$ charge distributions in PrBi at zero magnetic field. Calculated with $B_4=0.0012(2)$ K, and $B_6=-0.00065(3)$ K (or equivalently, $W=-0.8911$ K and $x=-0.0808$ in LLW parameters[36]). The quadrupolar moment operators are $\hat{O}_2^0=(3\hat{J}_z^2-\mathbf{J}^2)/2$, and $\hat{O}_2^2=\sqrt{3}(\hat{J}_x^2-\hat{J}_y^2)/2$.

$E(\text{K})$	0	0	50(5)	50(5)	50(5)	67(5)	67(5)	67(5)	122(5)
$ \ 4,+4\rangle$	0.0000	-0.5401	0.0000	0.0000	-0.7071	0.0000	0.0000	0.0000	0.4564
$ \ 4,+3\rangle$	0.0000	0.0000	-0.3236	-0.1425	0.0000	0.0000	0.6677	0.6551	0.0000
$ \ 4,+2\rangle$	-0.7071	0.0000	0.0000	0.0000	0.0000	0.0000	0.4952	-0.5047	0.0000
$ \ 4,+1\rangle$	0.0000	0.0000	-0.3771	0.8561	0.0000	-0.3536	0.0000	0.0000	0.0000
$ \ 4,\ 0\rangle$	0.0000	0.6455	0.0000	0.0000	0.0000	0.0000	0.0000	0.0000	0.7638
$ \ 4,-1\rangle$	0.0000	0.0000	-0.8561	-0.3771	0.0000	0.0000	-0.2524	-0.2476	0.0000
$ \ 4,-2\rangle$	-0.7071	0.0000	0.0000	0.0000	0.0000	0.0000	-0.4952	0.5047	0.0000
$ \ 4,-3\rangle$	0.0000	0.0000	-0.1425	0.3236	0.0000	0.9354	0.0000	0.0000	0.0000
$ \ 4,-4\rangle$	0.0000	-0.5401	0.0000	0.0000	0.7071	0.0000	0.0000	0.0000	0.4564
$\langle \hat{J}_z \rangle$	0.0000	0.0000	-0.3375	0.3375	0.0000	-2.5000	1.2738	1.2262	0.0000
$\langle \hat{O}_2^0 \rangle$	-4.0000	4.0000	-7.0000	-7.0000	14.0000	2.0000	-0.9428	-1.0572	-0.0000
$\langle \hat{O}_2^2 \rangle$	0.0000	0.0000	-8.9452	-8.9452	0.0000	0.0000	0.0000	-0.0000	0.0000
$\hat{\rho}_{4f}(\mathbf{r})$									

$x=-0.0808$ in Lea-Leask-Wolf (LLW) parameters[36]. This fitting confirms Γ_3 as the ground doublet, and the first excited state is Γ_4 triplet that sits at ~ 50 K above Γ_3 , cf the lower inset to Fig. 3. The energy level, wave function and the $4f$ charge distribution of each state are summarized in Table 1. The two ground states can be expressed in terms of $\Gamma_3^{(1)}=-\sqrt{\frac{1}{2}}|+2\rangle-\sqrt{\frac{1}{2}}|-2\rangle$, and $\Gamma_3^{(2)}=-\sqrt{\frac{7}{24}}|+4\rangle+\sqrt{\frac{5}{12}}|0\rangle-\sqrt{\frac{7}{24}}|-4\rangle$. We further calculated the dipolar moment ($\langle \hat{J}_z \rangle$) and quadrupolar moments ($\langle \hat{O}_2^0 \rangle$ and $\langle \hat{O}_2^2 \rangle$) carried by each CEF state, where $\hat{O}_2^0=(3\hat{J}_z^2-\mathbf{J}^2)/2$, and $\hat{O}_2^2=\sqrt{3}(\hat{J}_x^2-\hat{J}_y^2)/2$. Both $\Gamma_3^{(1)}$ and $\Gamma_3^{(2)}$ have zero $\langle \hat{J}_z \rangle$ and $\langle \hat{O}_2^2 \rangle$, but non-zero $\langle \hat{O}_2^0 \rangle$. This manifests that the ground doublet is nonmagnetic (i.e., non-Kramers) in nature, and is consistent with the fact that $\chi(T)$ levels off at low temperature. The Γ_3 doublet ground state with non-zero $\langle \hat{O}_2^0 \rangle$ can be further

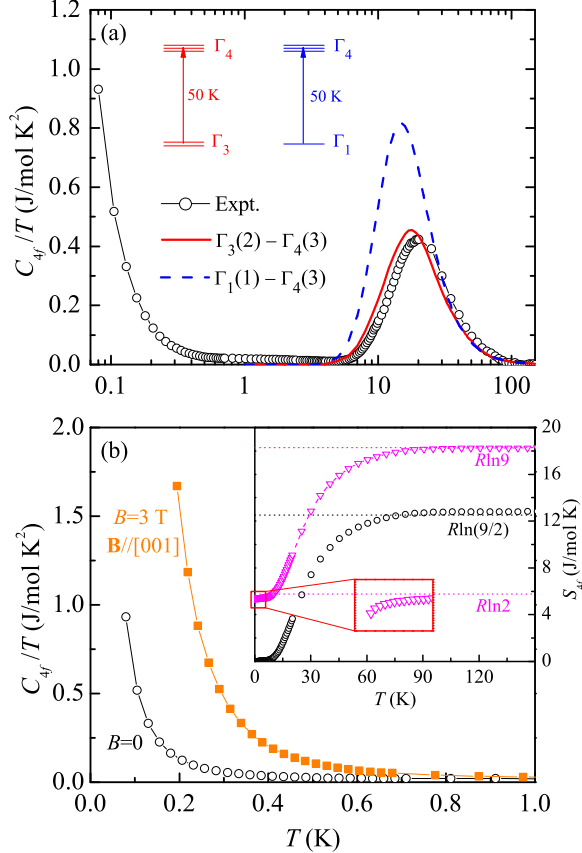


FIG. 4: **Specific heat of PrBi.** (a) Temperature dependence of C_{4f}/T , the $4f$ contribution to specific heat. The red-solid and blue-dash lines are calculated Schottky anomalies based on two distinctive CEF splittings (see the inset). (b) The C_{4f}/T of PrBi at low temperature, under $B=0$ and 3 T. The inset shows the integrated entropy S_{4f} ; the black circles are calculated by assuming $S_{4f}(2\text{K})=0$, and this leads to $S_{4f}\approx R \ln(9/2)$ at high T ; the magenta triangles represent an inferred curve with an assumption that the degeneracy of Γ_3 doublet is further lifted by a low- T quadrupolar ordering, so that S_{4f} exhibits a plateau of $R \ln 2$ and finally reaches $R \ln 9$ at high T .

evidenced by the anisotropic field dependent isothermal magnetization $M(B)$ as shown in the upper inset to Fig. 3. Note that the magnetic response to an external field generally is isotropic for a cubic system. The observed anisotropy is because the $\langle \hat{O}_2^0 \rangle$ order parameter gives rise to an additional field-induced $\langle \hat{J}_z \rangle$ component under $\mathbf{B} \parallel [001]$; such an induced component is expected to be weaker for $\mathbf{B} \parallel [011]$, and should be absent for the $\langle \hat{O}_2^2 \rangle$ order parameter with any field direction[12]. Similar anisotropy was also seen in other Pr-based intermetallic compounds such as $\text{PrIr}_2\text{Zn}_{20}$ *et al*[13, 14]. This CEF analysis also derives a small exchange field parameter $\lambda=-0.11 \text{ mol/emu}$, which agrees well with the small θ_W and

is suggestive of weak exchange interaction between local moments.

In Figure 4, we display the specific heat of PrBi. To start with, the specific heat of the non-4f analog LaBi at low temperature obeys the classic formula $C_{La}=\gamma_{La}T+\beta_{La}T^3$ (data not shown), with Sommerfeld coefficient $\gamma_{La}\approx1$ mJ/mol·K². Such a small γ_{La} is in consistency with the semimetallic nature. After subtracting C_{La} from the total specific heat of PrBi, we obtain the contribution from 4f electrons, C_{4f} . We show C_{4f}/T as a function of T in Fig. 4(a). A broad peak can be seen at around 25 K, which should be attributed to the Schottky anomaly due to CEF splitting. The peak position also suggests that the first excited level should be about 50 K above the ground state. We simulated the Schottky anomaly specific heat by considering Γ_3 or Γ_1 (both are nonmagnetic) as ground state, and the results are depicted as the red-solid and blue-dash lines in Fig. 4(a), respectively. This confirms the Γ_3 doublet as the ground state. We then derived the entropy by integrating C_{4f}/T over T from 2 K to 150 K. The entropy gain saturates at $R \ln(9/2)$ at high temperature, and this provides additional evidence for Γ_3 doublet as the CEF ground state, and moreover, this degeneracy remains un-lifted down to 2 K. We did not see the $R \ln(5/2)$ plateau, probably because the energy levels of Γ_4 and Γ_5 are too close.

It is possible that the degeneracy of the Γ_3 doublet ground state can be further lifted by quadrupolar Kondo effect or forming a quadrupolar ordering at lower temperature. To clarify this issue, we measured the specific heat down to 0.08 K with Dilution Refrigerator. A striking feature is that C_{4f}/T increases rapidly below 0.1 K. Such an increase does not conform to a $-\log T$ or T^{-3} behavior, which excludes Kondo effect or nuclear Schottky anomaly as an origin[8, 37]. Actually, both ¹⁴¹Pr (nuclear spin ¹⁴¹I=5/2) and ²⁰⁹Bi (²⁰⁹I=9/2) sit in local cubic-site symmetry with vanishing electric field gradient, the zero-field nuclear Schottky anomalies of them should be pushed to $T=0$. Since the CEF ground state is a nonmagnetic Γ_3 doublet, magnetic transitions are not likely, but rather quadrupolar transitions. Under magnetic field $\mathbf{B}\parallel[001]$, this anomaly moves to higher temperature [cf Fig. 4(b)]. This rules out a superconducting transition but is compatible with the quadrupolar ordering as seen in PrTm₂X₂₀[13, 15]. Note that an external magnetic field along [001] induces a dipolar component that can promote a quadrupolar ordering[38]. However, we should also mention that this field effect on the low- T specific heat probably have been exaggerated by the hyperfine-enhanced nuclear Schottky anomaly[37]. Because this quadrupolar phase transition is just below the base

temperature of our measurements, we are not able to calculate the entropy. An inferred $S_{4f}(T)$ at zero field can be given that it restores $\sim R \ln 2$ above the transition temperature and finally will saturate to $R \ln 9$ at high temperature, see the inset to Fig. 4(b). To achieve the $R \ln 2$ entropy gain, the jump in C_{4f}/T has to be extremely large at the transition (Note [39]). Clearly, the low temperature specific heat of PrBi requires further investigations.

DISCUSSION

To summarize the important findings:

- (1) By ultrahigh field quantum oscillation measurement, we confirm PrBi as a topological semimetal with low carrier density, $n_e + n_h \approx 8.6 \times 10^{20} / \text{cm}^3$, viz 0.06 /f.u.;
- (2) The $\text{Pr}^{3+} 4f^2$ sitting in the cubic-symmetry CEF has a nonmagnetic Γ_3 doublet ground state that carries non-zero $\langle \hat{O}_2^0 \rangle$ quadrupolar moments. They are expected to be ordered below 0.08 K;
- (3) Both quadrupolar Kondo effect and RKKY interaction seem to be rather weak in PrBi.

Expanding further on point (3) above. The weak RKKY interaction between the quadrupolar moments can be seen not only from the super low quadrupolar transition temperature, but also indicated by the small Weiss temperature θ_W and exchange-field parameter λ . As RKKY interaction relies on conduction electrons, it is reasonable that it is weakened in the case of low carrier density. Kondo effect is reduced, as well. 0.06 /f.u. means 6 conduction electrons are to separately screen 100 quadrupolar moments, which apparently is not enough[18]. In PrBi, although quadrupolar Kondo effect and RKKY interaction are both reduced, the latter appears to slightly win, which leads to the quadrupolar ordering as the ground state.

Topology, thus, meets active quadrupolar degrees of freedom in this low-carrier-density semimetal. It opens a new window to the physics of topology and strongly correlated effect with quadrupolar degrees of freedom. One interesting question is how does the physical property evolve with the *c-f* hybridization. We should point out that the $\text{Pr}Pn$ family ($Pn = \text{P,As,Sb,Bi}$) all crystallize in cubic structure and are all likely of Γ_3 CEF ground state. From Bi to P, the *c-f* hybridization should increase due to the “chemical pressure” effect, the low-temperature property may change. But meanwhile, the spin-orbit coupling reduces, and the topological feature probably fades out. This trend has been seen in the non-4f analog $\text{La}Pn$ [24, 40]. Another means is physical pressure effect, the advantages of

which are to maintain the spin-orbit coupling and to introduce little impurity or disorder. According to the well-known Doniach phase diagram[7], the Kondo effect increases faster than the RKKY interaction as c - f hybridization strengthens, we expect the quadrupolar ordering to be suppressed, quadrupolar fluctuations to proliferate as approaching some critical point, and more intriguing phenomena like heavy-fermion effect, non-Fermi liquid and/or unconventional superconductivity may emerge. Moreover, it is worthwhile to emphasize that low carrier density itself affects the character of quantum critical points. Our previous study on the (dipolar) Kondo semimetal $\text{CeNi}_{2-\delta}\text{As}_2$ tuned by pressure effect has manifested that unconventional Kondo-breakdown type quantum critical point[3, 41] is more likely to take place in the low carrier density limit[42]. Apart from these, it is also of great interest to see whether the topological feature switches if the CEF ground state is changed, e.g. tuned by uniaxial stress. We look forward to these peculiar phenomena in Pr-based semimetals. More experimental and theoretical works are needed in the future.

CONCLUSIONS

In all, the topological semimetal PrBi provides an interesting paradigm of quadrupolar degrees of freedom in the limit of low carrier density, evoking the necessity to revisit the Nozières exhaustion problem in the context of multi-channel Kondo effect.

Note added: When completing this work, we became aware of several publications on the MR and SdH effect of PrBi[22, 23].

METHODS

High quality single crystalline PrBi and its non-4 f reference LaBi were grown by Sb-flux method as described elsewhere[22–24]. Transport measurements were made in a standard Hall-bar configuration in a commercial Physical Property Measurement System with a rotator option (PPMS-9 T, Quantum Design). Magnetic susceptibility is measured in a Magnetic Property Measurement System (MPMS, Quantum Design) equipped with a vibrating sample magnetometer (VSM). The specific heat measurements were performed by a thermal relaxation method down to 0.08 K in a Dilution Refrigerator insert of PPMS. Magnetoresistance was also measured under pulsed magnetic field up to 53 T at Wuhan National High Magnetic Field Center.

First-principles calculations based on density functional theory (DFT) were performed

using the plane-wave basis projected augmented wave (PAW) method as implemented in Vienna Abinit Simulation Package (VASP)[43]. The Pr-4*f* orbitals were regarded as local core-states that provide the quadrupole instead of valence electrons, and do not explicitly enter the calculations. The energy-cutoff was chosen to be 480 eV, and a $12 \times 12 \times 12$ Γ -centered \mathbf{k} -mesh was used to converge the total energy to 1 meV per unit cell. The modified Becke-Johnson (mBJ)[44] was employed to obtain the electronic structure, which is then fitted using the maximally localized Wannier function method[45] to obtain the Fermi surface properties as well as the quantum oscillation frequencies.

Data availability

The authors declare that all source data supporting the findings of this study are available within the paper.

ACKNOWLEDGEMENTS

Y. Luo thanks Roman Movshovich, Joe D. Thompson and Stuart Brown for helpful discussions. This work is supported by the National Science Foundation of China (Grant nos. 51861135104, 11574097 and 11874137), National Key Research and Development Program of China (Grant no. 2016YFA0401704), Fundamental Research Funds for the Central Universities (Grant no. 2019kfyXMBZ071) and China Postdoctoral Science Foundation (2018M630846). S. Wang, Z. Zhu and Y. Luo acknowledge 1000 Youth Talents Plan of China.

AUTHOR CONTRIBUTIONS

Y.Luo conceived the project and designed the experiments. X.He synthesized the material and performed most of the measurements with assistance from C.Zhao, H.Yang, J.Wang, K.Cheng, S.Jiang, L.Zhao, Y.Li, S.Wang, Z.Zhu and L.Li. C.Cao carried out first-principles calculations. X.He and Y.Luo analyzed the data, discussed the results and wrote the paper with input from all the authors.

ADDITIONAL INFORMATION

Competing interests: the Authors declare no Competing Financial or Non-Financial Interests.

Publisher's note: Springer Nature remains neutral with regard to jurisdictional claims in

published maps and institutional affiliations.

- [1] Kondo, J. Resistance Minimum in Dilute Magnetic Alloys. *Prog. Theor. Phys.* **32**, 37-49 (1964).
- [2] Hewson, A. C. *The Kondo problem to Heavy Fermions.* (Cambridge University Press, Cambridge, UK, 1993).
- [3] Coleman, P. Dimensions are critical. *Nat. Mater.* **11**, 185-187 (2012).
- [4] Ruderman, M. A. & Kittel, C. Indirect Exchange Coupling of Nuclear Magnetic Moments by Conduction Electrons. *Phys. Rev.* **96**, 99-102 (1954).
- [5] Kasuya, T. A Theory of Metallic Ferro- and Antiferromagnetism on Zener's Model. *Prog. Theor. Phys.* **16**, 45-57 (1956).
- [6] Yosida, K. Magnetic Properties of Cu-Mn Alloys. *Phys. Rev.* **106**, 893-898 (1957).
- [7] Doniach, S. The Kondo lattice and weak antiferromagnetism. *Physica B+C* **91**, 231-234 (1977).
- [8] Cox, D. L. Quadrupolar Kondo effect in uranium heavy-electron materials? *Phys. Rev. Lett.* **59**, 1240-1243 (1987).
- [9] Cox, D. L & Makivic, M. Phenomenology of two channel Kondo alloys and compounds. *Physica B* **199-200**, 391-395 (1994).
- [10] Levy, P. M., Morin, P. & Schmitt, D. Large Quadrupolar Interactions in Rare-Earth Compounds. *Phys. Rev. Lett.* **42**, 1417-1420 (1979).
- [11] Onimaru, T. et al. Observation of Modulated Quadrupolar Structures in PrPb_3 . *Phys. Rev. Lett.* **94**, 197201 (2005).
- [12] Sato, T. J. et al. Ferroquadrupolar ordering in $\text{PrTi}_2\text{Al}_{20}$. *Phys. Rev. B* **86**, 184419 (2012).
- [13] Onimaru, T. et al. Antiferroquadrupolar Ordering in a Pr-Based Superconductor $\text{PrIr}_2\text{Zn}_{20}$. *Phys. Rev. Lett.* **106**, 177001 (2011).
- [14] Onimaru, T. et al. Simultaneous superconducting and antiferroquadrupolar transitions in $\text{PrRh}_2\text{Zn}_{20}$. *Phys. Rev. B* **86**, 184426 (2012).
- [15] Sakai, A. & Nakatsuji, S. Kondo Effects and Multipolar Order in the Cubic $\text{PrTr}_2\text{Al}_{20}$ ($\text{Tr}=\text{Ti}, \text{V}$). *J. Phys. Soc. Jpn.* **80**, 063701 (2011).
- [16] Tsujimoto, M. et al. Heavy-Fermion Superconductivity in the Quadrupole Ordered State of

- PrV₂Al₂₀. *Phys. Rev. Lett.* **113**, 267001 (2014).
- [17] Matsubayashi, K. et al. Heavy-Fermion Superconductivity in the Quadrupole Ordered State of PrV₂Al₂₀. *Phys. Rev. Lett.* **109**, 187004 (2012).
- [18] Nozières, P. Some comments on Kondo lattices and the Mott transition. *Phys. J. B* **6**, 447-457 (1998).
- [19] Sarrao, J. L. et al. Physical properties of Yb_XCu₄ (X =Ag,Au,Cd,Mg,Tl, and Zn) compounds. *Phys. Rev. B* **59**, 6855-6866 (1999).
- [20] Lawrence, J. M. et al. Slow crossover in Yb_XCu₄ (X =Ag,Cd,In,Mg,Tl,Zn) intermediate-valence compounds. *Phys. Rev. B* **63**, 054427 (2001).
- [21] Hasegawa, A. Fermi Surface of LaSb and LaBi. *J. Phys. Soc. Jpn.* **54**, 677-684 (1985).
- [22] Vashist, A. et al. Fermi surface topology and large magnetoresistance in the topological semimetal candidate PrBi. *Phys. Rev. B* **99**, 245131 (2019).
- [23] Wu, Z. Z. et al. Probing the origin of extreme magnetoresistance in Pr/Sm mono-antimonides/bismuthides. *Phys. Rev. B* **99**, 035158 (2019).
- [24] Niu, X. H. et al. Presence of exotic electronic surface states in LaBi and LaSb. *Phys. Rev. B* **94**, 165163 (2017).
- [25] Ali, M. N. et al. Large, non-saturating magnetoresistance in WTe₂. *Nature* **514**, 205-208 (2014).
- [26] Luo, Y. et al. Hall effect in the extremely large magnetoresistance semimetal WTe₂. *Appl. Phys. Lett.* **107**, 182411 (2015).
- [27] Singleton, J. *Band Theory and Electronic Properties of Solids*. (Oxford University Press, UK, 2001).
- [28] Xiang, F. X. et al. Observation of topological transition of Fermi surface from a spindle torus to a torus in bulk Rashba spin-split BiTeCl. *Phys. Rev. B* **92**, 035123 (2015).
- [29] Klitzing, K. v., Dorda, G. & Pepper, M. New Method for High-Accuracy Determination of the Fine-Structure Constant Based on Quantized Hall Resistance. *Phys. Rev. Lett.* **45**, 494-497 (1985).
- [30] Murakawa, H. et al. Detection of Berry's Phase in a Bulk Rashba Semiconductor. *Science* **342**, 1490-1493 (2013).
- [31] Tanida, H. et al. Possible Low-Temperature Strongly Correlated Electron Behavior from Multipole Fluctuations in PrMg₃ with Cubic Non-Kramers Γ_3 Doublet Ground State. *J. Phys.*

- Soc. Jpn.* **75**, 073705 (2006).
- [32] Bauer, E. D. et al. Superconductivity and heavy fermion behavior in $\text{PrOs}_4\text{Sb}_{12}$. *Phys. Rev. B* **65**, 100506 (2002).
- [33] Bauer, E. & Rotter, M. *Properties and Applications of Complex Intermetallics*. (World Scientific Publishing, Singapore, 2010).
- [34] Takegahara, K., Harima, H. & Yanase, A. Crystal Electric Fields for Cubic Point Groups. *J. Phys. Soc. Jpn.* **70**, 1190-1193 (2001).
- [35] Stevens, K. W. H. Matrix Elements and Operator Equivalents Connected with the Magnetic Properties of Rare Earth Ions. *Proc. Phys. Soc. Sect. A* **65**, 209-215 (1952).
- [36] Lea, K. R., Leask, M. J. M. & Wolf, W. P. The raising of angular momentum degeneracy of f -Electron terms by cubic crystal fields. *J. Phys. Chem. Solids* **23**, 1381-1405 (1962).
- [37] Gopal, E. S. R. *Specific Heats at Low Temperatures*. (Plenum Press, New York, 1966).
- [38] Shiina, R., Shiba, H. & Thalmeier, P. Magnetic-Field Effects on Quadrupolar Ordering in a Γ_8 -Quartet System CeB_6 . *J. Phys. Soc. Jpn.* **66**, 1741-1755 (1997).
- [39] We failed to measure specific heat of PrBi for lower temperatures with PPMS, probably because C_{4f}/T is too large on the transition.
- [40] Yang, H. Y. et al. Extreme magnetoresistance in the topologically trivial lanthanum monopnictide LaAs . *Phys. Rev. B* **96**, 235128 (2017).
- [41] Si, Q. et al. Locally critical quantum phase transitions in strongly correlated metals. *Nature* **413**, 804-808 (2001).
- [42] Luo, Y. et al. Pressure-tuned quantum criticality in the antiferromagnetic Kondo semi-metal $\text{CeNi}_{2-\delta}\text{As}_2$. *Proc. Natl. Acad. Sci. USA* **112**, 13520-13524 (2015).
- [43] Kresse, G. & Hafner, J. Ab initio molecular dynamics for liquid metals. *Phys. Rev. B* **47**, 558-561 (1993).
- [44] Tran, F. & Blaha, P. Accurate Band Gaps of Semiconductors and Insulators with a Semilocal Exchange-Correlation Potential. *Phys. Rev. Lett.* **102**, 226401 (1993).
- [45] Mostofi, A. A et al. An updated version of wannier90: A tool for obtaining maximally-localised Wannier functions. *Comput. Phys. Commun.* **185**, 2309-2310 (2014).

Figures Legends:

Fig. 1 Electrical transport properties of PrBi. (a) Resistivity as a function of temperature, $\rho_{xx}(T)$, in the absence of magnetic field. (b) MR reaches 430,000% (20,000%) for field up to 53 T (9 T). (c) SdH oscillation in $\Delta\rho_{xx}$ as a function of $1/B$. The inset depicts the Landau-level fan plot. The intercept at infinite-field limit indicates non-trivial Berry phase. (d) FFT of dHvA and SdH oscillations of PrBi (blue) and LaBi (black). (e) SdH FFT of PrBi for various field orientations, $\mathbf{B}\perp\mathbf{I}$. The black lines are guide lines to the Fermi surface structure. The dotted line is speculated from DFT calculations[21]. (f) $\rho_{xx}(B)$ and $\rho_{yx}(B)$ measured at 2 K. The solid line represents the two-band fitting of $\rho_{yx}(B)$.

Fig. 2 Fermi surface of PrBi. (a) DFT calculated Fermi surface of PrBi. The Fermi surfaces are indexed as α (electron-type, ellipsoidal, at X), β (hole-type, spherical, at Γ), and γ (hole-type, star-shaped, at Γ), respectively. The angular dependence of Fermi surface cross-sections are shown in panels (b) and (c), from theoretical and experimental, respectively.

Fig. 3 Magnetic properties of PrBi. Temperature dependence of magnetic susceptibility of PrBi measured under $B=0.1$ T and $\mathbf{B}\parallel[001]$. The inverse of χ is shown in the right frame. The symbols stand for experimental data, while the solid lines are theoretically calculated results based on CEF theory. The lower inset depicts the CEF splitting of the $j=4$ multiplet. The upper inset displays the field dependent isothermal magnetization at 2 K for $\mathbf{B}\parallel[001]$ (red squares) and $\mathbf{B}\parallel[011]$ (blue diamonds), respectively.

Fig. 4 Specific heat of PrBi. (a) Temperature dependence of C_{4f}/T , the $4f$ contribution to specific heat. The red-solid and blue-dash lines are calculated Schottky anomalies based on two distinctive CEF splittings (see the inset). (b) The C_{4f}/T of PrBi at low temperature, under $B=0$ and 3 T. The inset shows the integrated entropy S_{4f} ; the black circles are calculated by assuming $S_{4f}(2K)=0$, and this leads to $S_{4f}\approx R \ln(9/2)$ at high T ; the magenta triangles represent an inferred curve with an assumption that the degeneracy of Γ_3 doublet is further lifted by a low- T quadrupolar ordering, so that S_{4f} exhibits a plateau of $R \ln 2$ and finally reaches $R \ln 9$ at high T .

Tables Legends:

Table. 1 CEF parameters, energy levels, wave functions and the $4f$ charge distributions in PrBi at zero magnetic field. Calculated with $B_4=0.0012(2)$ K, and $B_6=-0.00065(3)$ K (or equivalently, $W=-0.8911$ K and $x=-0.0808$ in LLW parameters[36]). The quadrupolar moment operators are $\hat{O}_2^0=(3\hat{J}_z^2-\mathbf{J}^2)/2$, and $\hat{O}_2^2=\sqrt{3}(\hat{J}_x^2-\hat{J}_y^2)/2$.